View metadata, citation and similar papers at core.ac.uk
brought to you by CORE
provided by Loughborough University Institutional Repository

AN ANALYSIS OF THE AIR-JET YARN-TEXTURING PROCESS PART II: EXPERIMENTAL INVESTIGATION OF THE AIR-FLOW

M. ACAR, R.K. TURTON and G.R. WRAY
Loughborough University, UK

ABSTRACT

An account is given of an experimental investigation of the characteristics of the air-flow in a scaled-up model of a currently used nozzle for the air-jet texturing of yarns. The flow was found to be supersonic, turbulent, and of a non-uniform profile. Flow visualizations of the undisturbed and disturbed flows made by using the actual-size nozzle provided evidence that challenges previously postulated mechanisms of loop formation based on shock waves.

INTRODUCTION

There is a lack of understanding of the air-texturing mechanism, and the existing postulated explanations fail to provide a satisfactory explanation of how the loop formation is achieved. The air-flow in the standard-core HemaJet was investigated by experimental means in order to gain a better understanding of the flow in these nozzles. A dynamically similar scaled-up model of the HemaJet was used in these experiments because the minute size of the texturing nozzle made the use of measuring probes impracticable.

The effects of diverging trumpet-shaped exits were also investigated, pressure distributions inside the nozzle were measured, and measurement of turbulence was attempted.

Experiments were limited to a maximum pressure of 700 kPa (abs), this being the highest pressure of the air supply available for the scaled-up model, but the results provided sufficient information to predict the flow properties at higher working pressures.

Shadowgraph and interferometer techniques were used to visualize the flow from the actual-size nozzle at pressures used in practice to demonstrate the shock waves and the effects of the filaments on them.

Investigations of the air-flow in the converging-diverging type Taslan nozzles were curtailed in order to avoid repeating the extensive research undertaken by Bock and Luenenschloss[1-3].

The following nomenclature will be used:

a = acoustic speed;
cp = specific heat at constant pressure;
Cv = specific heat at constant volume;
L = characteristic length;
(*Ma)* = Mach number;
p = absolute static pressure;
P_0 = absolute stagnation pressure;
R = gas constant for a specific gas;
(Re) = Reynolds number (= $LV(\rho/\mu)$;
T = absolute temperature;
T_0 = absolute stagnation temperature;
V = velocity magnitude;
y = specific-heat ratio (= Cp/Cv);
p. = absolute or dynamic viscosity;
Q = density;

subscripts:

m = model;
p = prototype.

SCALING-UP THE NOZZLE

The main duct of the actual-size standard HemaJet is about 25 mm long and its diameter is 2 mm. The throat diameters of all three inlet bores are 0.9 mm. These inlet bores are radially equispaced, slightly staggered longitudinally, and situated nearer to the yarn-exit end rather than to the feed end, and they make an angle of approximately 48° to the axis of the main duct. The exit part of the nozzle is divergent, with trumpet-shaped curved walls.

The information obtained from the experiments with a model should be representative of that provided by the original system (prototype). From the dynamical-analysis standpoint, correct modelling is achieved if the conditions in the model are such that they are dynamically similar. Dynamic similarity exists when the model and the prototype each have the same length-scale ratio (geometric similarity), time-scale ratio (kinematic similarity), and force-scale or mass-scale ratio (dynamic similarity).

In the air-jet texturing process, the only predominant force acting on the filaments is the drag force. Drag force in general is a function of Reynolds number, *(Re),* and Mach number, (Ma). Any dynamic similarity will therefore result from the similarity of friction force (resistance) and the force stemming from the compressibility of the fluid (elasticity), characterized by:

$$(\varrho VL/\mu)_p = (Re)_p = (Re)_m = (\varrho VL/\mu)_m \quad (1)$$

and

$$(V/a)p = (Ma)p = (Ma)m = (V/a)m, \quad (2)$$

where the subscripts p and m denote the prototype and model, respectively. The Mach number becomes of paramount importance in high-speed compressible flows, as in the texturing nozzles, where density variations become significant. In such cases, the equalities of both Reynolds numbers and Mach numbers for the prototype and the model

are not possible, and only the equality of Mach numbers ($(Ma)_p = (Ma)_m$) needs to be considered for dynamically similar modelling of this high-speed compressible flow from texturing nozzles;

Since air at room temperature is the working fluid for both the prototype and the model, acoustic speeds ($a = (\rho RT)^{1/2}$) for both systems must be the same for the same operating pressures at room temperature, i.e., $a_P = a_m$ and hence $V_P = V_m$. A geometrically similar model is therefore also dynamically similar to the prototype when they operate at the same pressure. Hence the velocities at corresponding points in both the prototype and the model are caused to be equal, i.e., the time-scale ratio is unity. For a chosen length-scale ratio, the force-scale (mass-scale) ratio is equal to the square of the length-scale ratio.

A length-scaling factor of 4 was chosen as a compromise between the need to keep the compressed-air consumption rate below the level that can be delivered by the installed compressor and the desire for a reasonably large model in order to reduce the interference effects of the measuring probes.

The work was mainly confined to the Heberlein standard core HemaJet, which is a typical example of an industrially used cylindrical-type texturing nozzle. The scaled-up model of the HemaJet nozzle is shown in Fig. 1. Since the common characteristic of all types of texturing nozzle is to create a supersonic, turbulent, asymmetric, and non-uniform flow, the outcome of the investigations can therefore be generalized to any type of texturing nozzle.

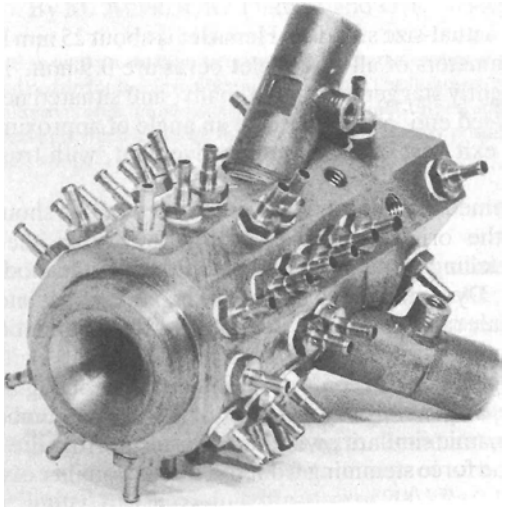

Fig. 1. Scaled-up model of the standard-core HemaJet

AXIAL-VELOCITY MEASUREMENTS

Experimental Details

The experimental rig as shown schematically in Fig. 2 was designed and built to facilitate velocity, turbulence, and static- and total-pressure measurements.

The fluid forces (drag forces) acting on the filaments are a function of the local air velocity; the distribution of the flow velocity at the exit region therefore plays an important role on the forces acting on the individual filaments, which will later be shown (in Part III) tube separated and dispersed in the nozzle[4].

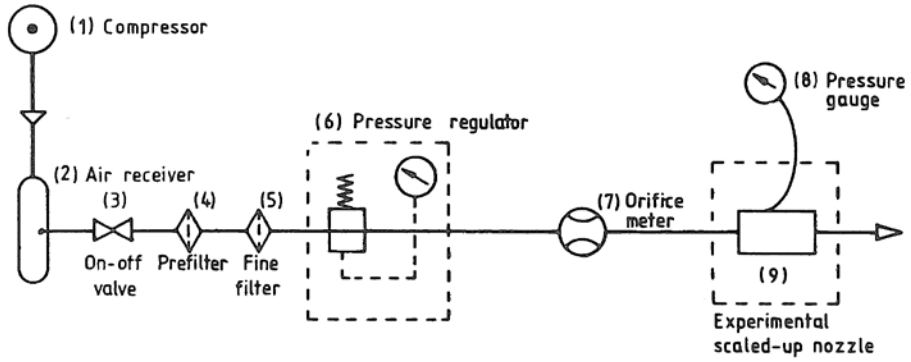

Fig. 2. Graphical representation of the experimental rig for the flow measurements

For the velocity measurements, constant-temperature heated-element anemometers (CTA) were first considered with miniature hot-wire and hot-film probes, but these had to be abandoned owing to the regular breakage of the wire and film elements after several measurements at very high flow velocities. A pitot-tube system was therefore used instead of the CTA system for the mean-axial-velocity measurements as described in Appendix A.

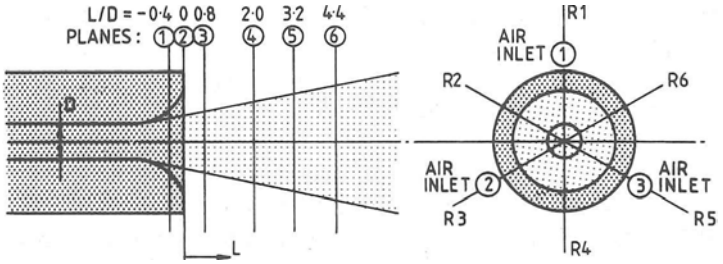

Fig.3. Vertical planes (1-6) to the nozzle axis and radial directions (R1-R6) at which the axial velocities were measured.

Axial-velocity Distribution

Velocities at three different planes in the exit region, i.e., at planes 1, 2, and 3, were each measured at six equispaced radial directions (as denoted in Fig. 3) at a working pressure of 600 kPa (abs). For this exit region, the velocity distributions show a slight axial asymmetry in the flow, as indicated in Table I. However, the degree of asymmetry, although it is shown to be higher towards the inside of the nozzle, is sufficiently low outside the nozzle to allow one to assume that the velocity distributions in any radial direction for any plane would represent the characteristics of the velocity distribution at that plane. Measurements in only one radial direction were therefore sufficient for further investigations of velocity distribution.

Fig. 4 illustrates the axial-velocity distributions at various planes situated at different distances away from the nozzle exit at 700 kPa (abs). It may be seen that substantial variations occur in the velocity distributions at planes near the nozzle exit; these have central depressions, and the maximum velocity occurs at approximately (3/4)r radial distance from the centre line, i.e., nearer to the nozzle walls.

Table I
Axial-velocity Distributions at 600 kPa at Planes 1, 2, and 3 for Equispaced Radial Directions Showing Slight Asymmetry

Radial Distance (mm)	Axial Velocity (m/s) at Radial Directions:					
	R1	R2	R3	R4	R5	R6
(a) At Plane 1						
0 (CL)	308	308	308	308	308	308
1	320	325	324	320	315	321
2	349	347	343	341	337	351
3	363	357	355	354	355	364
4	331	326	331	341	346	336
5	176	182	190	220	223	174
(b) At Plane 2 (Exit Plane)						
0 (CL)	338	338	338	338	338	338
1	345	348	347	343	340	347
2	363	361	359	356	354	365
3	370	367	363	366	367	373
4	324	324	333	343	350	326
5	187	204	221	238	246	198
6	47	66	81	104	99	58
(C) At Plane 3						
0 (CL)	351	351	351	351	351	351
1	353	354	351	351	354	354
2	358	356	357	355	355	355
3	343	343	348	351	355	355
4	288	293	303	318	327	327
5	200	216	224	247	255	255
6	109	126	137	159	159	159
7	47	41	66	81	74	74

It was shown by Wray[5] that longitudinal displacements occur between the filaments relative to each other. Since the fluid force acting on the scattered filaments is a function of the square of the local velocity, which depends on the position of the individual filaments within a nozzle, substantial variations occur in the drag force acting on these filaments, owing to their non-uniform velocity profile. It would therefore be expected that the scattered overfed individual filaments, each with an excess length free to be blown out by the air-flow, will travel at instantaneously different speeds, which are caused by the consider- able variations of the air velocity, and will be displaced longitudinally relative to each other.

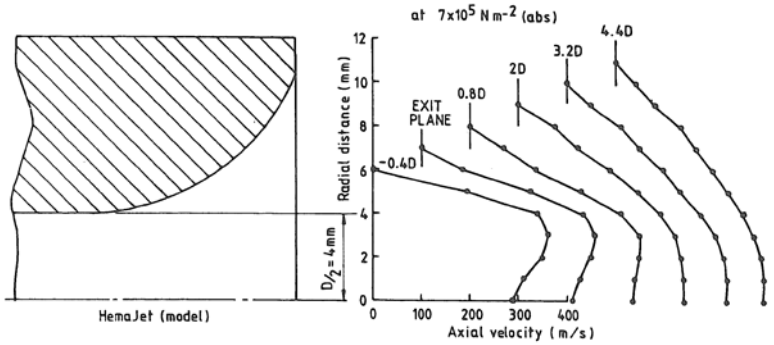

Fig. 4. Axial-velocity distributions from the HemaJet at 700 kPa (abs) at various planes

The effects of the working air pressure on the variations of the velocity distribution at the exit plane are shown in Fig. 5. The non-uniformity of the distribution, i.e., the central depression, becomes greater at higher pressures, and variation of the forces acting on the dispersed filaments across any one plane will therefore be greater than the corresponding force variations at lower pressures. These greater force variations result in-greater longitudinal displacements of the filaments.

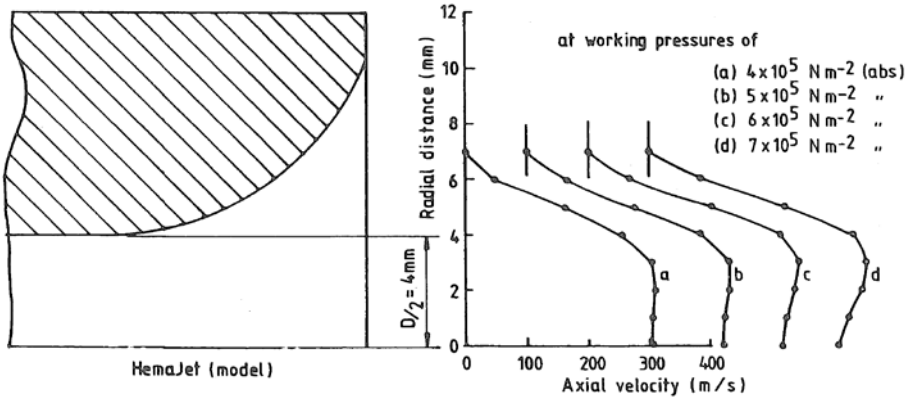

Fig. 5. Axial-velocity distribution from the HemaJet at the exit plane at various working pressures

Effects of the Trumpet-shaped Diverging Exit

The velocity distribution of the flow from the HemaJet is of a non-uniform profile (figures 4 and 5), whereas the velocity profile of the flow from the experimental cylindrical nozzle with a straight uniform main-flow duct (without a trumpet-shaped exit) is uniform, (Fig. 6(a)). The basic constructional differences between these two nozzles are that the HemaJet has a trumpet-shaped diverging exit and longitudinally staggered air-inlet bores. To analyse the causes of the non-uniform velocity distribution, the exit part of the cylindrical nozzle was modified to make it trumpet-shaped, similar to that of the HemaJet. Experiments with this nozzle showed that the exit-velocity distribution was non-uniform, with a central depression (Fig. 6(b)), similar to that of the HemaJet. Since the air-inlet bores in the experimental nozzle were not staggered, it

can therefore be concluded that this non-uniformity was caused by the trumpet-shaped diverging exit.

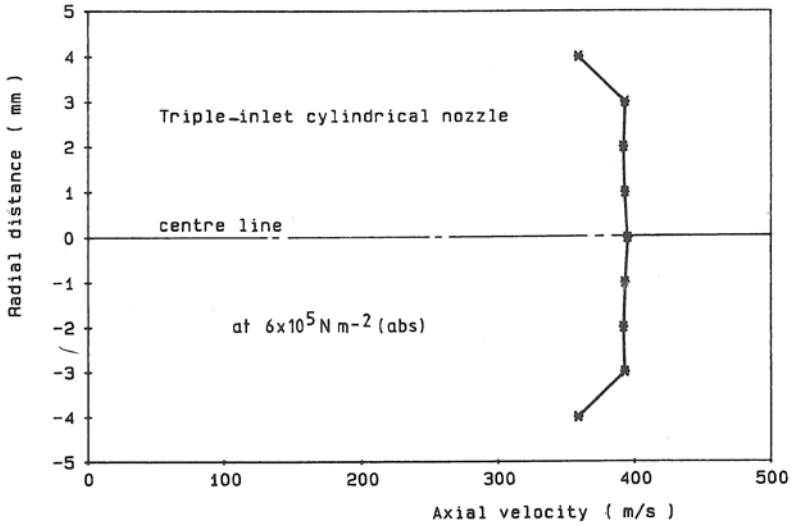

Fig. *6(a).* Axial-velocity distribution of the triple-inlet nozzle at the exit plane

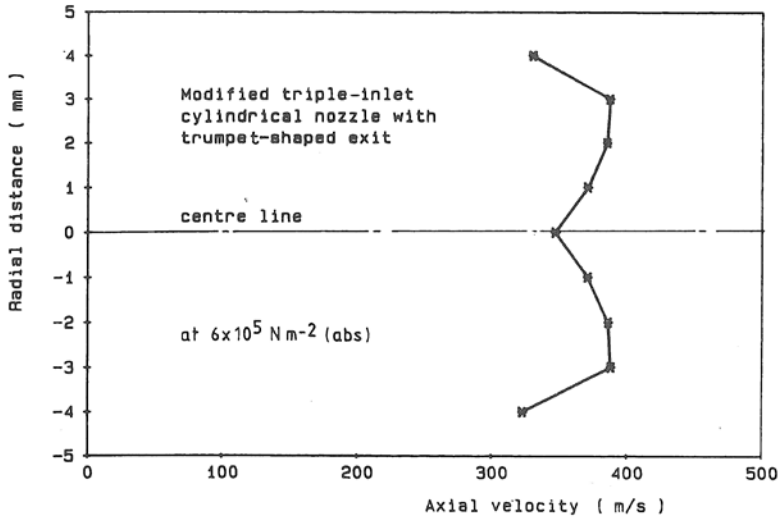

Fig.6(b). Velocity distribution at the exit plane of themodified triple-inlet cylindrical-type nozzle

Consequently , it can be argued that non-uniformity in the axial air-velocity distribution can be created or enhanced by modifying the exit of the cylindrical nozzles to a trumpet- shaped diverging exit. This may increase the differences in the magnitude of the forces acting on the filaments dispersed in the nozzle, which in turn enhance the longitudinal dis- placements of filaments relative to each other.

The staggered positions of the air-inlet bores induce a swirl to the flow. This swirl can be observed as the twist inserted in a bundle of stationary filaments placed in the nozzle.

Centre-line-velocity Variations by Distance

The variations of the centre-line velocity by distance from the exit plane of the HemaJet are shown in Fig. 7(a) for various pressures. A gradual drop of the centre-line velocity was observed after a slight initial rise, the maximum occurring at different distances from the nozzle exit for different pressures. This rise, which is more pronounced at higher pressures, may be due to very weak shock waves that are likely to occur in the flow.

The periodic rises and falls in the centre-line velocity are observable in the flow from a Taslan Type 14 nozzle, as shown in Fig. 7(b), which were not evident with the HemaJet at similar pressures. This is because of the stronger shock waves obtainable with converging- diverging nozzles (see Section 7). Consequently, it can be argued that weaker shock waves occur in the cylindrical type of HemaJet than in the converging-diverging type of Taslan nozzles.

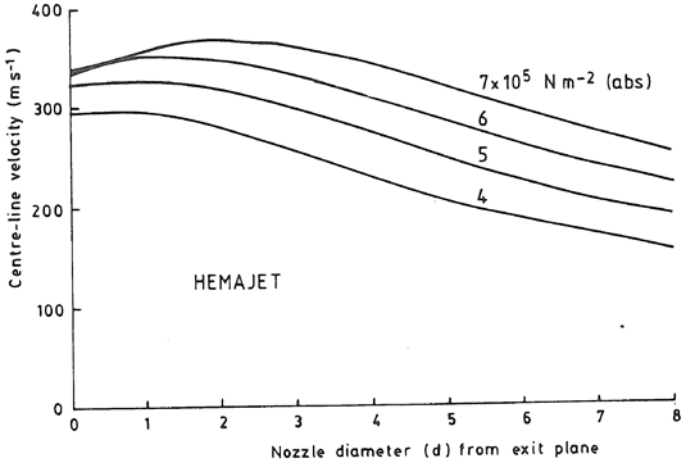

Fig. 7(a). Centre-line-velocity variations with distance from the HemaJet nozzle exit plane

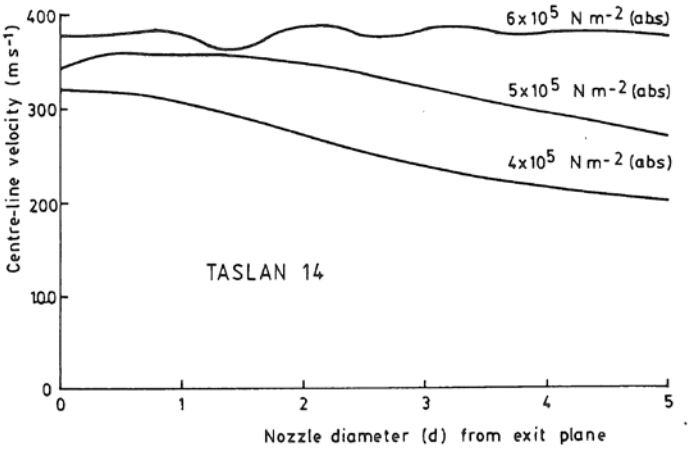

Fig. 7(b). Centre-line-velocity variations with distance from the Taslan Type 14 nozzle exit plane

TURBULENCE MEASUREMENTS

Wray and Entwistle[6], in their explanation of the mechanism of texturing,re erred to turbulence in the flow in a Taslan Type 9 nozzle, which was later experimentally verified by Sen[7]. Bock and Luenenschloss[1-3], although they did not give experimental evidence of the turbulence, referred to its role in the texturing process with a Taslan Type 14 nozzle.

In such high velocities provided by cylindrical nozzles, intense turbulence is expected. An attempt was made to measure it, but, because of the difficulties encountered in employing hot-wire anemometry (see Section 3.1), no satisfactory results were obtained. However, these preliminary trials indicated a typical turbulence level in the region of 25-30%. Observations of the filament behaviour, as will be described in Part III[4], also showed that intense turbulence occurs in such supersonic flows from a texturing nozzle. During texturing, this turbulence will contribute to the movement of the filaments across the nozzle,which will in turn cause further disturbances in the flow and hence increase the intensity of the turbulence. It is therefore believed that the turbulence and movements of the filaments could mutually contribute to each other's activity.

STATIC-PRESSURE M E A S U R E M E N T S

Because of the restricted accessibility, and the blocking effect of any velocity probe when used inside the nozzle, it was not practicable to measure the velocities, but a series of pressure tappings, as shown in Fig. 8, enabled the static pressures to be measured. These pressures were recorded at various distance planes along the nozzle axis and with up to twelve pressure tappings at each plane and are shown in Figures 9 and 10.

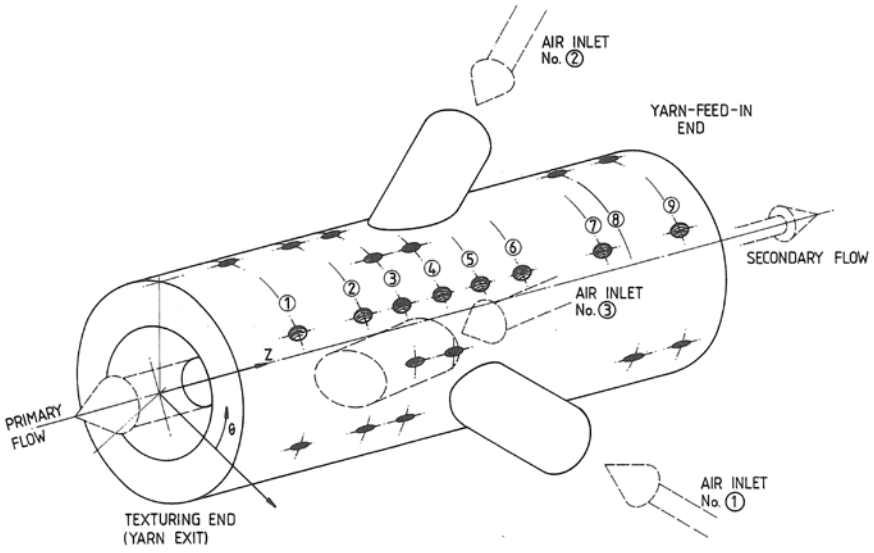

Fig. 8. Scaled-up model of the HemaJet, showing the positions of the pressure tappings

The results indicate that the static-pressure distribution inside the nozzle is asymmetric in the region of the air-inlet bores; as would be expected from the staggered positions of these inlets. The distribution of the pressure (Fig. 9) becomes more uniform and symmetrical towards the nozzle-exit region, and only a slight asymmetry remains in the flow out- side the nozzle, as was shown in Section 3.2.

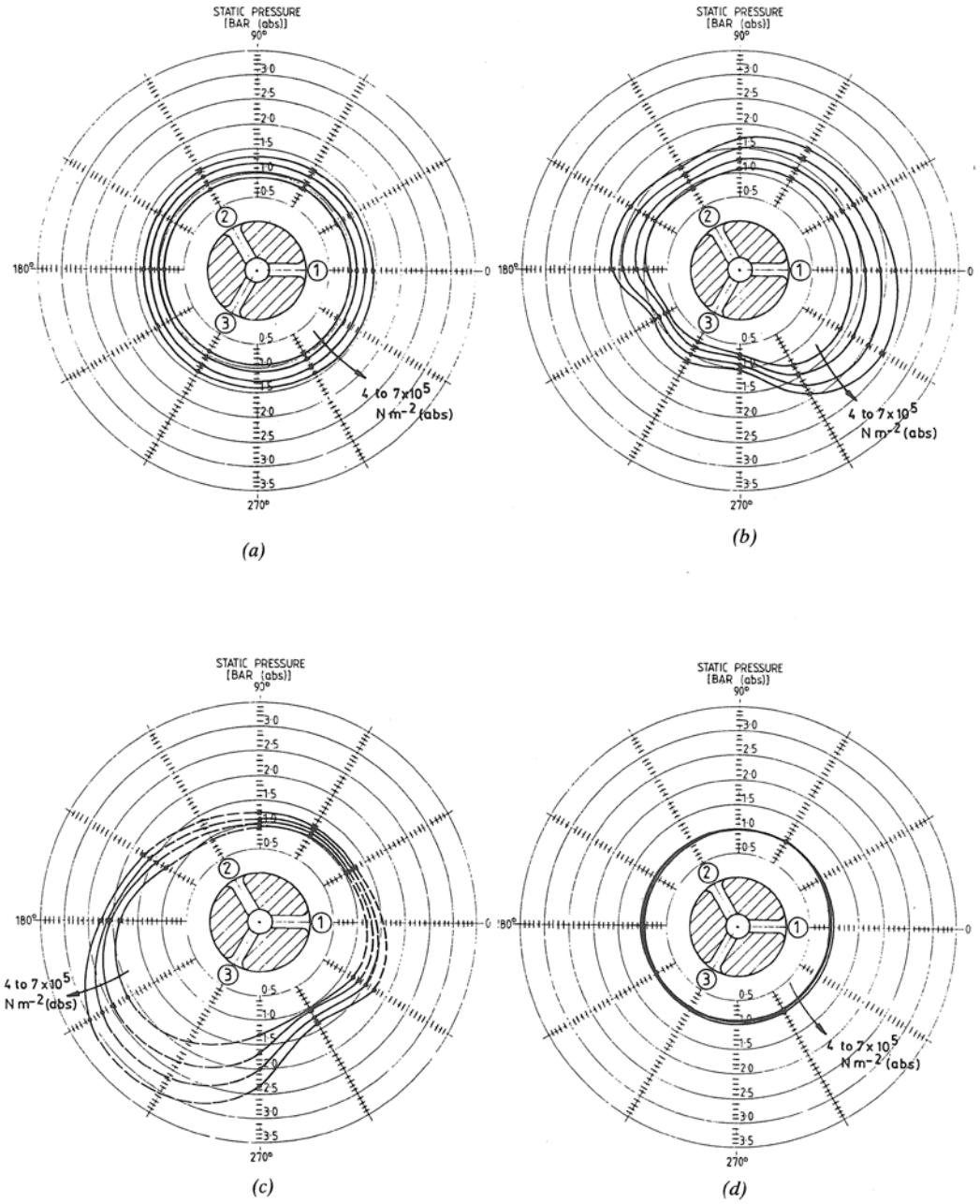

Fig. 9. Static pressures at planes, 2, 3, 4, and 5 as denoted in Fig: (a) plane 2, viewed from texturing end; (b) plane 3, viewed from texturing end; (c) plane 4, viewed from texturing end; (d) plane 5, viewed from texturing end (1 bar = 100 kPa = 10s Nm-2)

Although the static pressure drops towards the exit, it remains dependent on the upstream stagnation pressure, and it is above the atmospheric level for working pressures greater than 500 kPa (abs), as shown in Fig. 10. By contrast, for the secondary flow, it drops to atmospheric pressure rapidly, regardless of the upstream working pressure.

Supersonic flows from texturing nozzles, with static pressures above atmospheric nearer to the exit plane, obtainable at the practical working-pressure range, suddenly expand to the ambient atmospheric pressure and cause expansion waves as will be discussed in later.

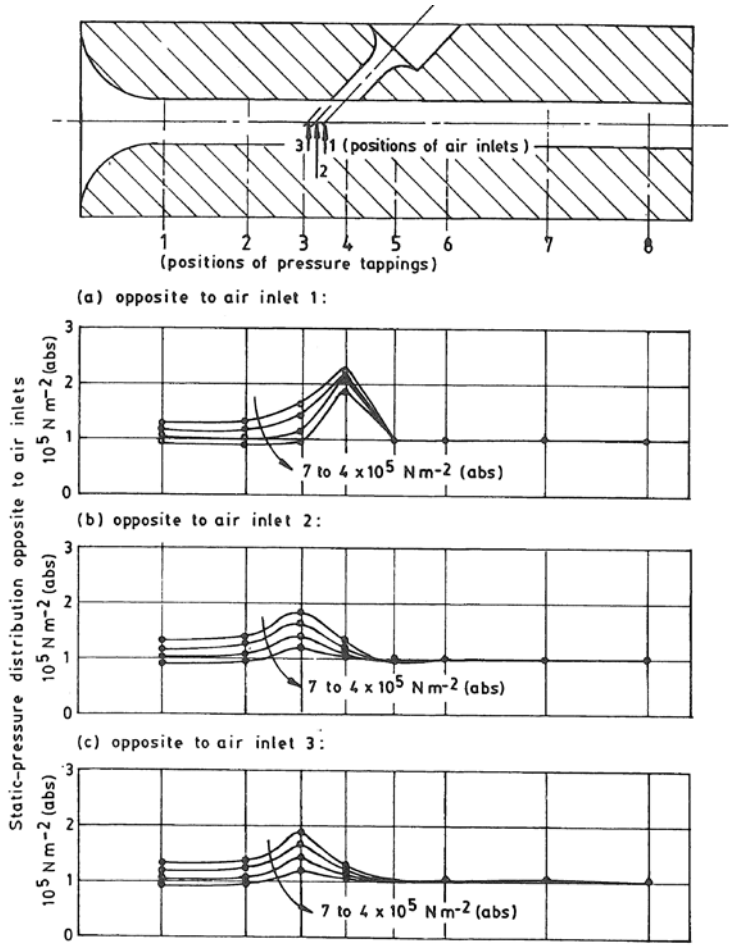

Fig. 10. Static-pressure distribution along the nozzle opposite to the air inlets

INTERACTIONS BETWEEN THE FILAMENTS AND THE AIR-FLOW

Attempts to measure the air velocity while the filaments were in the nozzle failed because of their interference with the measuring probes.

As will be shown in Part IV[8], homogeneously suspended particles mixed in an air-flow reduce the air velocity. In an air-jet texturing nozzle, the filaments are continuously present in the nozzle in a dispersed form. They, analogous to the particles, act so as to reduce the air velocity, because the momentum required to blow out the filaments is transferred from the air-flow alone.

As discussed by Wallis[9] in a gas-flow containing homogeneously suspended particles, if strong shock waves occur in the flow, the gas is suddenly decelerated across the shock to a lower velocity, while the particles enter this zone at their upstream velocities (Fig. 11).

Continuous filaments dispersed in the air-flow may behave in a manner similar to the particles in an air-flow, and their velocities may not be affected by the shock waves. In addition, since the larger portions of the filaments are still inside the nozzle and are under the effects of the higher velocities of the upstream flow, they may continue to travel at a speed induced by this flow.Hence, even if strong shock waves occur in the flow during texturing, it is very unlikely that these will serve to decelerate the filaments.

VISUALIZATIONS OF THE FREE AND DISTURBED FLOWS

Pressure Waves

Static-pressure measurements at plane 1, closest to the exit plane, as denoted in Fig. 8, indicated that the static pressures exceeded atmospheric at high working pressures.This means that the flow does not expand completely inside the nozzle and that this expansion occurs outside the nozzle in the form of successive expansion waves, where the pressure drops to ambient. Compression waves will be present when the exit pressure is lower than the ambient pressure, this pressure rising above the ambient after the shock wave and then repeating itself outside the nozzle in the form of expansion and compression waves through successive falls and rises of pressures until it completely expands into the ambient pressure.

Free Air-flow

Previous attempts by Sen[6], using a scaled-up model of a Taslan Type 9 nozzle in Perspex, failed to investigate the flow inside the nozzle because of the poor optical quality of the plastics material, particularly when used with circular cross-sections. However, he was able to obtain information regarding the pattern of the free flow outside the nozzle by Schlieren photography[7,10,11]. Later, Sivakumar[12] theoretically verified the existence of shock waves in a free flow from Taslan Type 9 and 10 nozzles at normal operating pressures. Bock and Luenenschloss[1-3] demonstrated the shock waves in a free flow from a Taslan Type 14 nozzle, also by using Schlieren photography.

A Michelson interferometer[13] and a laser shadowgraph system were used by the authors to investigate the nature of the free flow in the actual HemaJet nozzle rather than a scaled- up model. Fig. 12 shows the interferograms of the shock waves that occur in a high-speed compressible flow from the HemaJet texturing nozzle. These shock waves diminish at low pressures.

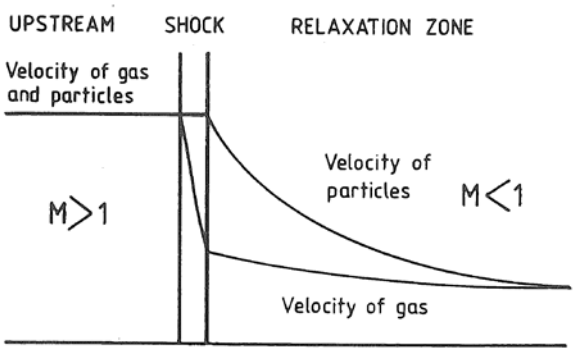

Fig. 11. Effects of shock waves on the gas and particle velocities in a gas-particles mixture flow (after Wallis[9])

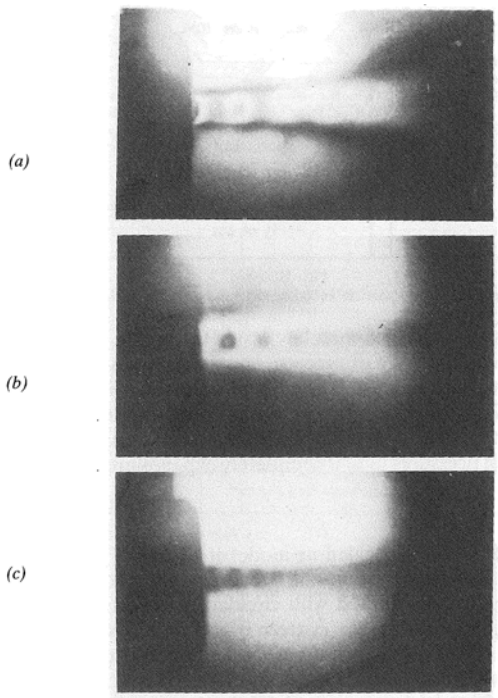

Fig. 12. Interferograms of the shock waves as affected by a spherical impact element (at *(a) 1000* kPa, *(b)* 800 kPa, and (c) 500 kPa)

Disturbed Air-flow

The most recently postulated mechanisms of loop formation have been based on shock waves[1-3]. The experiments on which these claims were based were apparently all con- ducted with an undisturbed free flow, i.e., without filaments being present in the nozzle. To investigate whether these were valid, shadowgraphs showing the shock waves in the flow were obtained while the filaments were in the nozzle, which thus simulated actual texturing conditions. Figures 13(a) and 14(a) show shadowgraphs for a free (undisturbed) flow from the

HemaJet and Taslan Type 14 nozzles, respectively. Figures 13(b) and 13(c) are shadow- graphs obtained from the HemaJet at the same working pressures, but with

filaments pre- sent in the nozzle, as observed from two different viewing angles. The dark areas are the shadows of the emerging filaments. Figure 14(b) and 14(c) show similar shadowgraphs for the Taslan Type 14 nozzle.

These shadowgraphs provide evidence to show that, whereas they can exist in the undisturbed flows, shock waves are destroyed in the flows disturbed by the filaments. Hence any mechanism of loop formation based on such shock waves and deceleration of the filaments owing to pressure barriers caused by these shock waves is very unlikely to be valid.

In addition, it is clear from Figures 13 and 14 that the shock waves from a HemaJet are not as strong as those from a Taslan nozzle. If shock waves are effective in loop formation, this ought to reduce their effects on the filaments and on the entire process of texturing; nevertheless, the HemaJet is at least as effective in texturing as the Taslan nozzle, and this throws doubt on the assumption that shock waves play a significant role in effective texturing.

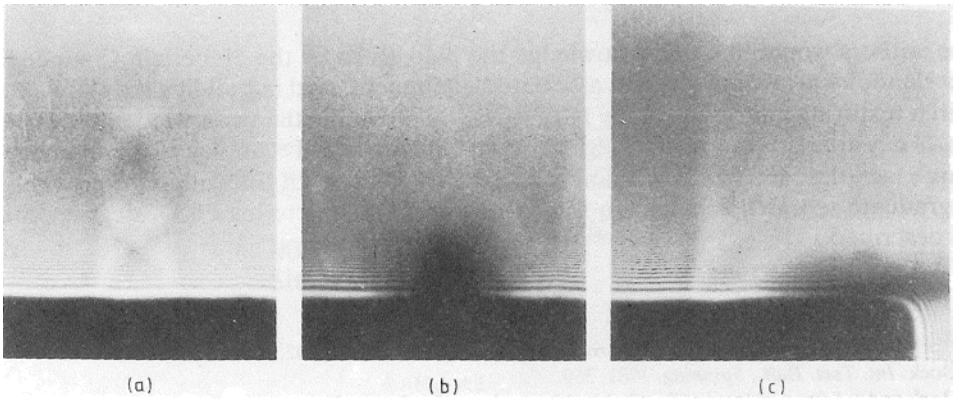

Fig. 13. Shadowgraphs of free and disturbed flows from a standard-core HemaJet, at 1000 kPa (abs)

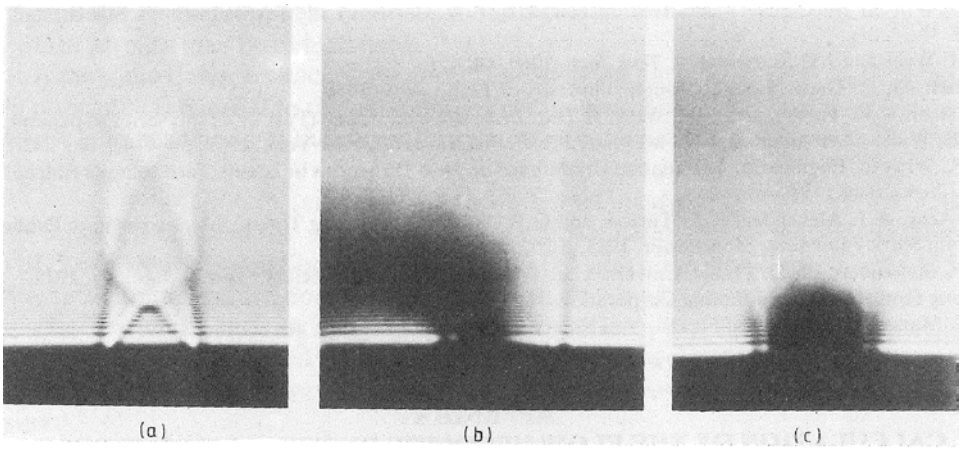

Fig. 14. Shadowgraphs of free and disturbed flows from a Taslan 14 nozzle, at 900 kPa (abs)

CONCLUSIONS

Axial-velocity measurements at the exit of the cylindrical-type HemaJet nozzles showed that the flow is supersonic, turbulent, slightly asymmetric, and of a non-uniform distribution. Similar results were obtained recently by other researchers[1-3], with converging- diverging-type Taslan nozzles, which thus confirms that these characteristics are fundamental to effective texturing.

Velocity and the degree of non-uniformity in the velocity distribution increase with the increasing pressure. Since the forces acting on the filaments are determined by the local flow velocity, the variation in the local velocity is an essential requirement of the texturing process, because this causes longitudinal displacements of the filaments relative to each other. High turbulence, as expected from the supersonic flow and from the complex design of the nozzle, also contributes to the movements of the filaments in the nozzle so as to interchange their dispositions within its cross-section.

Static pressures show that the flow in the nozzle near the air-inlet bores is very complex and contributes to the asymmetry and non-uniformity of the primary flow. Although the secondary-flow pressure drops to atmospheric, the primary-flow pressure, especially at higher working pressures (above approximately 500 kPa (abs)), stays above atmospheric at the exit of the nozzle, which causes expansion waves. Shock waves from a Taslan nozzle are much stronger than those from a HemaJet, even though the HemaJet is a very effective industrial texturing nozzle. These shock waves in free, undisturbed flows are destroyed by the filaments in the actual texturing process. This leads to the conclusion that the shock waves do not play any significant role in the texturing process.

ACKNOWLEDGEMENTS

The authors would like to acknowledge the help given by the Heberlein Company of Switzerland, by providing jets and associated equipment used in building the single-head research texturing machine, an\1 by ICI Fibres, by providing the yarns used in the experiments. They are also grateful to Loughborough University of Technology for providing the research facilities, and M.Acar thanks the Turkish Ministry of Education for providing a post-graduate research scholarship to enable him to complete his Ph.D. degree on the work described.

REFERENCES

1. G. Bock and J. Luenenschloss. *Chemifasern / Textilindustrie,* 1981, 31/83,202,380.
2. G. Bock. *Int. Text. Bull., Spinning,* 1981,359.
3. G. Bock and J. Luenenschloss in 'Textile Machinery: Investing for the Future', the Textile Institute, Manchester, 1982.
4. M. Acar, R.K. Turton, and G.R. Wray. *J. Text. lnst.,* to be published (Part III of this series of papers).
5. G .R. Wray in 'Bulk, Stretch, and Texture' (edited by P.W. Harrison), the Textile Institute, Manchester, 1966, p. 18.
6. G.R. Wray and J.H. Entwistle. *J. Text. Inst.,* 1969, 60,411.
7. H. Sen. Ph.D. Thesis, Loughborough University of Technology, 1970.

8. R M. Acar, R.K. Turton, and G.R. Wray. *J. Text. Inst.,* to be published (Part IV of this series of papers).
9. G. B. Wallis.'One-dimensional Two-phase Flow', McGraw-Hill, New York, 1969, pp. 1-43, 175-242.
10. G.R. Wray in 'Engineering Foundation Conference on New Directions in Textile Technology', Ringe, N.H., U.S.A., Aug., 1976.
11. M. Acar, A.J. Alexander, R.K. Turton, and G.R. Wray in 'Texturing Today', Shirley Institute Publication S46, Shirley Institute, Manchester, 1983. p.207.
12. V.R. Sivakumar. Ph.D. Thesis, University of Manchester Institute of Science and Technology, 1975.
13. Ealing Optics Catalogue, Ealing Corporation, 1981.
14. B.S. Massey. 'Mechanics of Fluids', Van Nostrand-Reinhold, London, 4th edition, 1979.

APPENDIX

CALCULATION OF THE FLOW VELOCITY BY USING PITOT TUBES IN SUBSONIC AND SUPERSONIC FLOWS

Stagnation pressures as measured by pitot tubes in subsonic and supersonic flows can be used to calculate flow velocities in the axial direction, as discussed by Massey[14] The pro- cess by which the fluid is brought to rest at the nose of a pitot tube is assumed to be friction- less and adiabatic. For subsonic flows (Fig. Al), then:

$$V_2/2 = C_p (T_0 - T) = C_p T_0 \{1 - (p/P_0)^{(\gamma - 1)/\gamma}\}. \qquad \text{(A.l)}$$

where the suffix 0 refers to stagnation conditions.

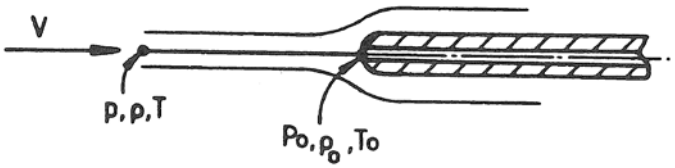

Fig. A1. Pitot tube in a subsonic flow

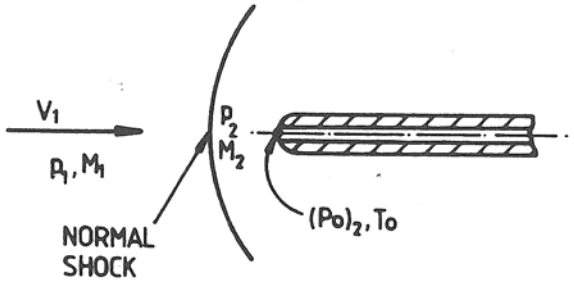

Fig. A2. Pitot tube in a supersonic flow *(M_1 = (Ma) 1, M_2 = (Ma) 2*

If T_0 and the ratio (p/P_0) of static to stagnation pressures are both known, then the velocity of the stream may be determined.

For supersonic flows, a shock wave forms ahead of the Pitot tube (Fig. A2). If the axis of the Pitot tube is parallel to the oncoming flow, the shock wave may be assumed normal to the stream line leading to the stagnation point; and the pressure rise across the shock is then given by:

$$(P_0)_2/p_1 = \{(\gamma+1)^{\gamma+1}/(2\gamma(Ma)_1^2-\gamma+1\}\{(Ma)_1^2/2\}^{(1/\gamma-1)} \quad \text{(A.2)}$$

This equation enables the upstream Mach number, $(Ma)_1$ to be calculated from the ratio of downstream stagnation pressure $(P_0)_2$ to, the upstream static pressure (p_1). Since the stagnation temperature does not change across the shock wave, we then have:

$$C_p T_0 = C_p T_1 + V_1^2/2 = C_p(V_1^2/\gamma R(Ma)_1^2) + V_1^2/2. \quad \text{(A.3)}$$

Thus V1 may also be calculated if T_0 is known. Hence the downstream stagnation pressure, $(P_0)_2$, stagnation temperature, T_0, and upstream static pressure, $P >$ are required to be measured.

In the application of this method to a free jet, when it -is not practicable to measure the static pressure, it can be assumed that the static pressure is atmospheric.